



CHORUS

This is the accepted manuscript made available via CHORUS. The article has been published as:

First-principles study of surface charging in $\text{LaAlO}_3/\text{SrTiO}_3$ heterostructures

K. Krishnaswamy, C. E. Dreyer, A. Janotti, and C. G. Van de Walle

Phys. Rev. B **92**, 085420 — Published 19 August 2015

DOI: [10.1103/PhysRevB.92.085420](https://doi.org/10.1103/PhysRevB.92.085420)

First-principles study of surface charging in LaAlO₃/SrTiO₃ heterostructures

K. Krishnaswamy

*Department of Electrical and Computer Engineering,
University of California, Santa Barbara, California 93106-9560, USA*

C. E. Dreyer, A. Janotti, C. G. Van de Walle

Materials Department, University of California, Santa Barbara, California 93106-5050, USA

The two-dimensional electron gas (2DEG) observed at the interface between LaAlO₃ (LAO) and SrTiO₃ (STO) is known to be very sensitive to the proximity of the LaAlO₃ surface and the conditions to which the surface is exposed. We use first-principles calculations to study surface reconstructions on LAO films, taking into account that the LAO surface can be charged. The results for the charged surfaces and for the coupling between the surface and the 2DEG enable us to account not only for the behavior of the 2DEG as a function of thickness of the LAO layer, but simultaneously determine the stable terminations and reconstructions on the LAO surface under a variety of conditions. Our studies of charged surfaces are based on an extension of the methodology of Lozovoi *et al.* [J. Chem. Phys. **115**, 1661 (2001)]. From the calculated electronic structure of the unreconstructed (but relaxed) AlO₂ and LaO surface terminations of LAO, we find surface states having excess holes (AlO₂ termination) or excess electrons (LaO termination). This result is central to understanding the mechanism of 2DEG formation, and is consistent with a 2DEG of density $3.3 \times 10^{14} \text{ cm}^{-2}$ being intrinsic to the LaO-TiO₂ interface in the LAO/STO system. We explore the effects of the Al-atom, O-vacancy and H-atom surface reconstructions on the 2DEG density, and find that the stability of different reconstructions is tied to the thickness of the LAO layer as well as the surface exposure conditions. We find that including the effects of charging of the surface significantly stabilizes the AlO₂ termination *versus* the LaO termination. Overall, our methodology has the advantage of decoupling first-principles calculations for the interface from those for the charged surface, and constitutes a general approach that can be applied to the commonly occurring problem of charge exchange between the surface and the interface of a thin film with a substrate, or between the surface and defects/impurities in the bulk of a material.

I. INTRODUCTION

Observations of a two-dimensional electron gas (2DEG) with high carrier density ($\sim 10^{13} \text{ cm}^{-2}$) [Refs. 1–4] at the (001) interface between SrTiO₃ (STO) and LaAlO₃ (LAO) have generated great interest. In spite of a decade of investigations, the mechanisms governing the 2DEG formation and its density are not yet fully understood. The polar catastrophe model^{1,5} is still widely used to explain interface doping in this heterostructure, although experimental evidence⁶ does not seem to support it. A complete and consistent model that can explain all the experimental findings in the LAO/STO heterostructures is still lacking.

Recent calculations^{7–11} as well as experiments^{12–15} have stressed the importance of the LAO surface in determining the density of the 2DEG at this interface. Cen *et al.*¹² demonstrated the reversible process of inducing conductivity at the LAO/STO interface using a conductive tip at the surface of LAO by applying a field. Other groups^{13–19} have observed similar phenomena and find a strong correlation between the environment to which the surface of LAO is exposed and the 2DEG density at the interface. Despite the important role played by the surface, there is a lack of experimental studies to determine the exact nature and structure of the LAO surface in this system. Most groups assume the surface to be AlO₂-terminated by counting RHEED intensity oscilla-

tions during growth.^{12,20} However, the surface termination and its structure may change upon exposure to conditions under which the 2DEG properties are measured.

It has been previously demonstrated that electrons residing in the 2DEG with a density of $3.3 \times 10^{14} \text{ cm}^{-2}$ ($0.5e^-$ per areal unit) are intrinsic to the interface between LAO and STO⁷ along the [001] direction. If the LAO layer is sufficiently thin, these electrons can transfer to empty surface states on the LAO surface and deplete the 2DEG density; indeed, the experimentally observed 2DEG densities are much lower than the nominal $3.3 \times 10^{14} \text{ cm}^{-2}$.^{2–4} Such a transfer of electrons from the interface also leaves the LAO surface charged. This phenomenon of surface charging is a common occurrence in many other systems of practical interest as well, but has not been addressed from first principles so far.²¹ It is the goal of the present study to rigorously address the physics involved with surface charging within a first-principles context, and apply the understanding to model the interactions between the interfacial 2DEG and the surface in LAO/STO heterostructures. We note that Bristowe *et al.*⁹ adopted an opposite viewpoint for the mechanism of 2DEG formation: they did not consider the 2DEG to be intrinsic to the LAO/STO interface, but assumed that the carriers appear at the interface in order to screen the field in the LAO. Although in the case of thin LAO films terminated by a surface both viewpoints are equivalent, the arguments in Ref. 9 break down in the case of a superlattice, or LAO capped with another material.

Most theoretical efforts to date have focused on studying the interface properties of the LAO/STO heterostructures.^{22,23} Surface studies for these heterostructures^{10,24} have been limited to a small set of surface structures owing to the high computational cost involved. We overcome this limitation by formulating a model that represents the coupling between the LAO surface and the LAO/STO interface, including the effects of surface charging. This allows us to calculate the properties of the LAO surface separately from those of the interface. We can then use the model to study the heterostructure as a whole. This approach eliminates the need for studying both STO and LAO (i.e., the interface and the surface) within the same calculation, thus greatly lowering the computational demand and allowing us to more thoroughly explore surface reconstructions. Even more importantly, the separation of the surface problem from the interface problem results in a more general formulation, which will be useful to address similar systems in the future. Bristowe *et al.*⁹ have proposed a model to consider O-vacancy defects on the surface, from the viewpoint that the carriers in the 2DEG arise in order to screen the field in LAO. Their model uses a number of parameters taken from different sources, and does not allow for a general comparison between different surface terminations with various defects. In our work we overcome this limitation by an explicit consideration of the absolute surface energy. There have been other proposed mechanisms for the origin of carriers at the interface, which are based on defects in STO bulk, cation intermixing, and oxygen vacancies near the interface.^{25–27} These issues will be not be dealt with in this paper.

In order to study the surface of LAO as a separate entity, and to include the effects of charging the surface, calculations that treat charged surfaces of a dielectric are required. The usual theoretical treatment of surface reconstructions assumes that the surfaces always remain neutral. Indeed, the computational treatment of non-neutral surfaces has not been possible in the past, since a non-neutral system clearly leads to divergences in energy, and robust methods for providing charge neutralization in the case of semiconductors or insulators were lacking.²⁸ Charged surfaces do occur, however, in many situations of practical interest. One example is the surfaces of doped semiconductors, which typically exhibit band bending in the near-surface region. Depletion of carriers leads to fixed charge and the formation of a space-charge region, and the free carriers charge the surface by occupying surface states.^{29,30} The amount of band bending is determined by Fermi-level pinning at the partially filled surface states. In the case of semiconductor surfaces, the amount of surface charge is typically small relative to the density of atoms on the surface. In contrast, in the LAO/STO system the amount of charge transferred to the surface (0.5 electrons per areal unit cell) is of the order of the surface atomic density. Due to the magnitude of the amount of charge added to the sur-

face, careful treatment of the charged surface is essential to accurately address the energetics.

In this work, we determine the stable surface terminations and reconstructions of LAO films grown on STO substrates. This is accomplished by first calculating surface energies of various surface reconstructions and terminations on the (001) surface of LAO, using first-principles calculations based on hybrid density functional theory, taking into account the effects of charging the surface. Subsequently, the system consisting of a thin LAO film on an STO substrate is analyzed, allowing us to examine the interplay between LAO thickness, density of the 2DEG at the LAO/STO interface, and the stability of surface reconstructions on the LAO surface. We consider Al-atom, H-atom and O-vacancy reconstructions, which can be regarded as corresponding to a high density of point defects on the surface. We will also investigate the consequences of modifying the density of such point defects. While we do not explicitly calculate isolated surface defects, but estimate the energetics based on reconstructions with varying coverage, we will use the term “surface defects” to refer to a uniformly spaced 2D array of defects (such as Al-adatoms) with a given concentration. Overall, our interest will be to quantify the 2DEG density remaining at the LAO/STO interface after the transfer to the surface, that would minimize the total energy of the system for a certain thickness of LAO, and result in a stable LAO surface.

The paper is organized as follows: In Sec. II A we describe our first-principles calculations to determine atomic and electronic structure as well as energetics of surfaces. Section II B describes the methodology involved in calculating the surface energies of neutral reconstructed as well as unreconstructed LAO surfaces from first principles. The approach developed by Lozovoi *et al.*³¹ to treat charged surface of metals is generalized to the treatment of charged surface of dielectrics, as systematically explained in Sec. II C. In Sec. III, we calculate and discuss the electronic structure of the bulk and the surface of LAO. In Sec. IV we build on the methodology of Sec. II C and the results of Sec. III to formulate a model for the surface energetics of LAO in LAO/STO heterostructures, i.e., in the presence of an interfacial 2DEG. By applying the model to various surface reconstructions, we can determine the most stable surface termination as well as stable surface reconstructions. Finally, in Sec. V, we discuss the 2DEG density at the LAO/STO interface for surfaces of LAO with varying densities of Al-atom, H-atom and O-vacancy surface defects. Based on the results obtained for the 2DEG density, the trends related to the thickness of LAO films are discussed for a variety of environmental conditions to which the surface might be exposed.

II. METHODOLOGY

A. First-principles method

Our first-principles calculations were performed using density functional theory (DFT) with the screened hybrid functional of Heyd, Scuseria and Ernzerhof (HSE),^{32,33} and the projector augmented wave method^{34,35} as implemented in the Vienna *Ab-initio* Simulation Package (VASP).^{36–38} The use of the HSE hybrid functional with the default mixing parameter α of 25% gives an accurate description of the band gap and lattice parameters of both LAO and STO.^{39,40}

In order to study surfaces, we used the supercell approach with a symmetric slab geometry based on cubic LAO with a slab thickness of 5.5 unit cells corresponding to 11 layers of LAO with two identical surface terminations along the [001] direction, separated by ~ 15 Å of vacuum [see Fig. 1(a)]. Each layer corresponds to a plane of atoms, either an AlO₂-plane or an LaO-plane [See also Sec. III]. Therefore, a supercell having an AlO₂-terminated surface will have 6 layers of AlO₂ and 5 layers of LaO. Our supercells contain only an LAO slab along with vacuum, and do not include STO or any interfaces. We therefore do not explicitly address the electrons in the 2DEG, but focus on the surface properties of LAO, for which the HSE functional provides accurate results.⁴¹ Three layers at the center of the slab were kept fixed to the LAO bulk structure, while atoms within two unit cells (4 layers) of each surface were allowed to relax. Due to the periodic boundary conditions there may be interactions between the periodic images of the surfaces. We have explicitly verified, by independently varying the slab thickness and vacuum thickness, that our geometry leads to results that are converged to within 0.35 meV/Å². For bulk calculations, integrations over the Brillouin zone used a Monkhorst-Pack⁴² k -point mesh of $4 \times 4 \times 4$, while a $4 \times 4 \times 1$ mesh was used for the (1×1) surface calculations, and a $2 \times 2 \times 1$ mesh for the (2×2) surface calculations. The area of a (1×1) unit cell is 14.29 Å².

B. Surface energy of neutral reconstructed LaAlO₃ surfaces

The surface energy can be determined from supercell calculation for a slab with the equation:

$$\gamma_{\text{surface}} = \frac{1}{2} [E_{\text{slab}}(n_{\text{LAO}}) - E_{\text{bulk}}(n_{\text{LAO}}) - n_{\text{La}} \cdot \mu_{\text{La}} - n_{\text{Al}} \cdot \mu_{\text{Al}} - n_{\text{O}} \cdot \mu_{\text{O}}], \quad (1)$$

where E_{slab} is the total energy of the slab supercell containing two identical surfaces, $E_{\text{bulk}}(n_{\text{LAO}})$ is the total energy of the corresponding number of bulk LAO cells, n_i is the number of excess atoms of species i in the slab supercell, and μ_i is the chemical potential of species i , which is a variable representing experimental conditions.

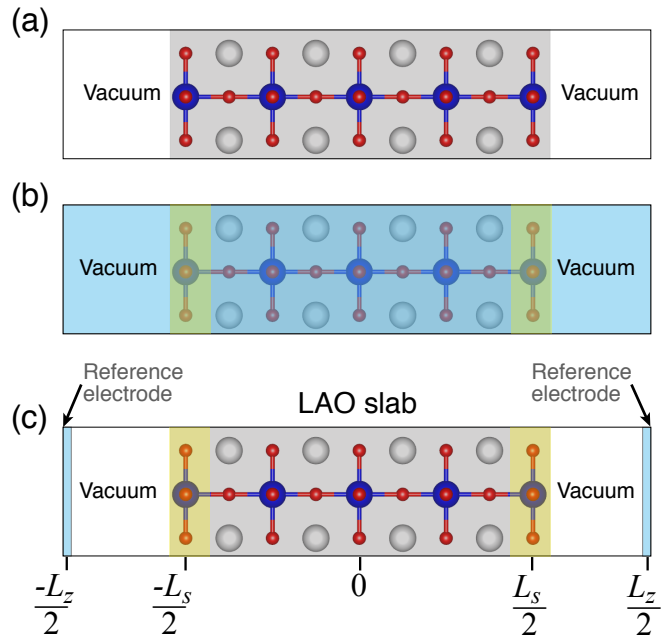


Figure 1. (Color online) Schematic illustration of (a) the supercell used to calculate a symmetric neutral slab with dielectric constant ϵ with vacuum on either side, (b) the process of adding charge (shown in yellow) to the surface of the slab with a uniform compensating background charge (shown in blue) spread throughout the supercell, and (c) an auxiliary system with reference electrodes at the cell edges.

The stability equation of LAO, expressed in terms of the chemical potentials μ_i of the constituent elements referenced to their elemental phases, is:

$$\mu_{\text{Al}} + \mu_{\text{La}} + 3\mu_{\text{O}} = \Delta H_f(\text{LaAlO}_3), \quad (2)$$

where $\Delta H_f(\text{LaAlO}_3)$ is the enthalpy of formation of LAO. The formation of competing phases such as Al₂O₃ in the Al-rich limit, and La₂O₃ in the La-rich limit, imposes additional constraints:

$$\text{Al-rich: } 2\mu_{\text{Al}} + 3\mu_{\text{O}} \leq \Delta H_f(\text{Al}_2\text{O}_3), \quad (3)$$

$$\text{La-rich: } 2\mu_{\text{La}} + 3\mu_{\text{O}} \leq \Delta H_f(\text{La}_2\text{O}_3), \quad (4)$$

where $\Delta H_f(\text{Al}_2\text{O}_3)$ and $\Delta H_f(\text{La}_2\text{O}_3)$ are the enthalpies of formation for Al₂O₃ and La₂O₃, respectively.

C. Methodology to treat charged surfaces

The first-principles method to obtain surface energies described above applies to neutral surfaces. Adding charge to a slab supercell creates serious complications, which have stymied calculations for charged 2D systems in the past: since the energy of an infinite, periodic, charged system diverges, the added charge must be compensated so the periodically repeated supercell is overall

charge neutral. The issue of charge compensation has been thoroughly studied in the case of point defects in the bulk, where charge compensation is provided by a uniform compensating background charge (CBC), and rigorous prescriptions have been formulated for extrapolating to the dilute limit.^{43–45} Applying a CBC over the entire supercell is, in practice, achieved simply by removing the $\mathbf{G} = 0$ term in the Fourier expansion of the electrostatic potential.

In the case of charged surfaces, two complications arise. Applying a uniform CBC to the entire supercell may create artifacts, since the presence of a uniform charge in the vacuum region is unphysical. The second complication is that, because of the varying dielectric profile the screening of the CBC is different in different regions of the supercell. In the case of point defects on the surface, where the main focus is on removing spurious interactions between defects in neighboring cells in order to determine results for the dilute limit, specific prescriptions have been formulated to correct the calculated energies.²⁸

In our present system, however, we are interested not in the dilute limit, but in situations where the concentration of charge on the surface may be on the order of the atomic density. Overall charge neutrality could of course be achieved by calculating the complete system, i.e., including the LAO/STO interface in the supercell;^{10,46,47} however, as discussed in the introduction, this would require treatment of a system with a very large number of atoms, exceeding what can be addressed with hybrid density functional calculations. More importantly, it is not clear how one would disentangle the properties of the interface and the surface, making it difficult to discuss the physics and also to present the results in a form that can productively be used for further analysis of similar systems (e.g., with different layer thicknesses). Instead, we focus on calculations for a charged LAO slab with a uniform CBC, and correct for spurious effects by adopting a methodology originally developed by Lozovoi *et al.*³¹ for charged metal surfaces, which we generalize here for the case of a dielectric slab.

The approach is illustrated schematically in Fig. 1. The actual DFT calculations are performed for a charged slab in a compensating background [Fig. 1(b)], but we will use post-processing corrections to convert the energies and electrostatic potentials to those of an auxiliary system consisting of the charged slab compensated by grounded metal “reference electrodes” at the supercell boundaries.³¹ This allows us to separate the electrostatic effects associated with the addition of surface charge from the changes in surface energy. The purpose of introducing the “reference electrodes” in the auxiliary system is two-fold: (1) to prevent the divergence of the electrostatic potential due to the charged slab (same role as a compensating charge), and (2) to serve as a consistent reference for the comparison of the energies of surfaces with different charges. The electrodes do not contribute to the energy of the cell as they are infinitely thin, but they determine the value (set to zero) of the electrostatic

potential at the boundaries. Relaxation of the atomic positions in a charged supercell could be performed in principle by relaxing the structure based on forces that are appropriately corrected to remove the spurious effect of the CBC. However, such force corrections have not yet been addressed.^{28,31} In the present work we fix the structure to correspond to that of the neutral (relaxed) structure, and neglect any relaxations that may result from charge addition.

The methodology to compute the energy of charged surfaces involves three steps. First, we calculate the total energy and the macroscopic average of the electrostatic potential energy of a slab cell with charged surfaces and a CBC. Second, we correct the macroscopically averaged electrostatic potential energy and the total energy of the slab by removing the contributions from the homogeneous background charge. As the final step, we separate out the surface-energy change due to the addition of charge, by referencing to the neutral surface.

In the following discussions, the symbol V (in units of Volts) will consistently be used to refer to electrostatic *potential*, to be distinguished from the electrostatic *potential energy* that electrons experience. Since electrons have negative charge (with magnitude e), this potential energy corresponds to $-eV$ (in units of eV).

1. Macroscopic averaging

We first calculate and extract the surface energy of the neutral surface, using the supercell approach described in Sec. II A. As the surface is perpendicular to the z direction of the supercell, for the quantities of interest such as the charge density and the electrostatic potential energy, it is useful to obtain the *xy planar average* (PA) and consequently, the one-dimensional *macroscopic average* (MA), which is a running average over a period of the lattice.⁴⁸ An example for the PA and MA of the electrostatic potential energy (in units of eV) obtained from our first-principles calculation is shown in Fig. 2 for a neutral surface terminated by an AlO_2 plane. Note the constant value of the MA potential energy in the vacuum region as well as in the center of the slab region between the two surfaces. This constant value is reached already within two atomic distances from the surface. This rapid convergence is reassuring with regard to the ability of the supercell geometry to capture the results for an isolated surface, avoiding any spurious interactions between the two slab surfaces.

2. Removing the contributions due to the background charge

The electrostatic potential calculated from first principles can be written as a superposition:

$$\tilde{V}(r) = V(r) + V_b(r) \quad (5)$$

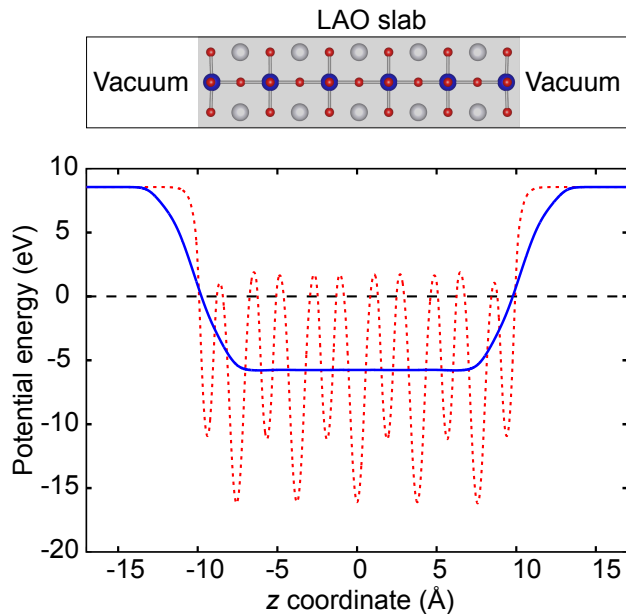


Figure 2. (Color online) Averaged electrostatic potential energy in a supercell containing a slab of LAO with unreconstructed neutral (relaxed) AlO_2 -terminated surfaces. The dotted (red) line corresponds to the planar average of the potential energy in the xy plane; the solid (blue) line is the one-dimensional macroscopic average. The dashed (black) line indicates the average of the electrostatic potential energy taken over the entire supercell, which is arbitrarily set to zero here (a common convention in first-principles calculations). The top panel shows the geometry of the supercell, aligned to the plot of the potential energy.

where $\tilde{V}(r)$ is the electrostatic potential of the slab supercell including the CBC, $V_b(r)$ is the electrostatic potential of the CBC, and $V(r)$ is the quantity we want, namely the electrostatic potential of the charged slab supercell *without* the CBC.

In order to obtain an expression for $V_b(r)$, we make the approximation, as proposed by Komsa and Pasquarello,²⁸ that the electrostatics of the slab supercell can be represented by a *macroscopic* dielectric profile $\varepsilon(z)$ that varies only in the z direction. Within this approximation we can easily solve for the electrostatic potential contribution from the CBC, $V_b(z)$, using the Poisson equation:

$$\frac{d}{dz} \left(\varepsilon(z) \frac{d}{dz} V_b(z) \right) = -\rho_b = -\frac{q}{\Omega}, \quad (6)$$

where q is the total CBC and Ω is the volume of the supercell.

In order to define the boundary conditions in solving for $V_b(z)$ from the Poisson equation in Eq. (6), and also to pick a suitable reference potential for comparing systems with different amounts of charge, grounded “reference electrodes” are placed at the cell boundaries. We assume that these reference electrodes are far enough

from the slab that the only contribution to the potential at that distance is from $V_b(z)$. Since the reference electrodes are grounded, this gives us the boundary conditions, $V_b(\pm L_z/2) = 0$, to solve the Poisson equation.

To further simplify the analysis, we approximate the dielectric profile to be a piecewise constant function with relative dielectric constant ε in the slab and unity in the vacuum. Since we neglect relaxations, ε is taken to be the “clamped ion” static dielectric constant (electronic part of the static dielectric constant). For LAO, we use $\varepsilon = 4.0$ [Ref. 49]. The approximation of a piecewise constant function requires defining a boundary. We choose the boundary to correspond to the atomic positions of the outermost surface layer. Solving the Poisson equation gives

$$V_b(z) = \frac{-q}{2\varepsilon_0\Omega} \times \begin{cases} \left(z^2 - \frac{L_z^2}{4} \right), & -L_z/2 < z < -L_s/2 \\ \frac{1}{\varepsilon} \left(z^2 + \frac{L_s^2}{4} (\varepsilon - 1) - \varepsilon \frac{L_z^2}{4} \right), & -L_s/2 < z < L_s/2 \\ \left(z^2 - \frac{L_z^2}{4} \right), & L_s/2 < z < L_z/2. \end{cases} \quad (7)$$

Equation (7) is a generalization of the results for a metallic slab obtained by Lozovoi *et al.*³¹ to the case of a dielectric slab; the equations for a metal slab can be recovered by taking the limit $\varepsilon \rightarrow \infty$.

Using Eq. (7) for V_b , we can obtain the corrected electrostatic potential $V(r)$ from the calculated uncorrected potential $\tilde{V}(r)$ using Eq. (5). The corrected and uncorrected electrostatic potential energies (which differ by a factor of $-e$ from the electrostatic potential), for the case of $0.25e^-$ added per areal unit cell, are plotted in Fig. 3 along with the potential energy due to the CBC, $-eV_b(z)$. In this figure, all the potential energies are shifted by a constant such that their value at $\pm L_z/2$ is set to zero, as required by the placement of the reference electrodes. The discontinuity in the slope of $-eV_b(z)$ at $\pm L_s/2$ is due to our choice of the dielectric profile to be piecewise constant. The corrected potential energy has some key features that illustrate the procedure involved in removing the contribution from the CBC. $-eV_b(z)$ has a smaller curvature within the slab compared to the vacuum region due to the screening present in the slab. Comparing the profiles of the corrected and uncorrected potential energies within the slab region, we see that the correction removes the parabolic contribution that is present in the uncorrected potential energy due to the presence of the uniform CBC; the corrected potential energy is flat (corresponding to zero electric field) in the interior of the slab. Similarly, the uncorrected potential energy has a curvature in the vacuum region, again due to the presence of the uniform CBC; after correction the potential energy becomes linear in the vacuum region. This linear potential profile is equivalent to the potential drop across a parallel-plate capacitor, with the reference electrode forming one of the plates, and the sheet of excess

surface charge forming the other plate. The slope of the potential (in units of $V/\text{\AA}$), which gives the field, is positive in the left vacuum region. This situation corresponds to a sheet of positive charges on the reference electrode, and a sheet of negative charges on the surface, indeed consistent with our addition of $0.25e^-$ per areal unit cell to the surface, compensated by countercharges on the reference electrodes.

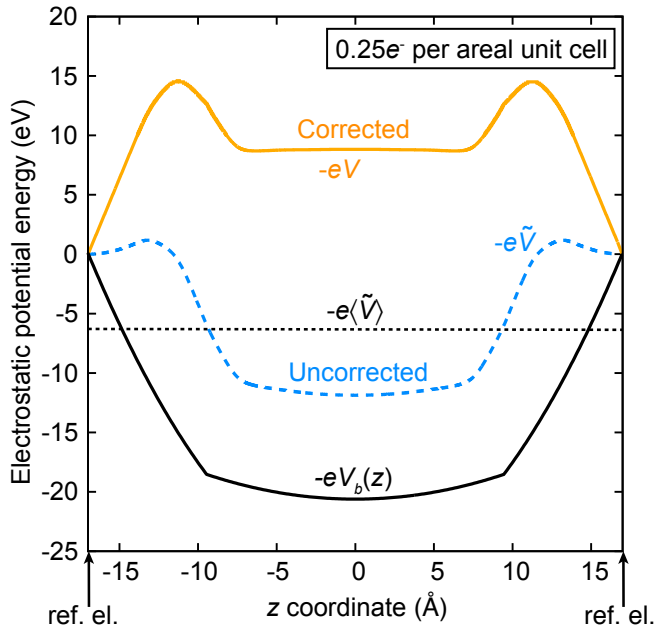


Figure 3. (Color online) Electrostatic potential energies in a supercell containing a slab of LAO with unreconstructed AlO_2 -terminated surfaces, to which a charge of $0.25e^-$ per areal unit cell is added. The calculated uncorrected electrostatic potential energy (labelled $-e\tilde{V}$) shifted to set the value at $\pm L_z/2$ (supercell boundaries) to 0 eV, is shown by the dotted (blue) curve. The electrostatic potential energy corrected by removing contributions due to CBC (labelled $-eV$) is shown by the solid light (orange) curve, and the potential energy due to the CBC is shown as solid black curve. The average value of the uncorrected potential energy, labeled $-e\langle\tilde{V}\rangle$, is shown by the dotted horizontal line. The positions of the reference electrodes are indicated by arrows and labeled “ref. el.”.

It is important to check the sensitivity of the results to the specific details of the approach, namely the shape of the dielectric profile and the placement of the surface plane, $L_s/2$. As will be reported in Sec. IV C, we found that the specific choices made here have only minimal effects on the final surface energies.

For completeness, we should acknowledge that Eq. (5), which was our starting point, involves an assumption, namely that we can define the electrostatic potential of the charged slab supercell *without* the CBC by subtracting the contributions due to the CBC [$V_b(r)$] from the electrostatic potential obtained directly from the first-principles calculation [$\tilde{V}(r)$]. In principle, the ground-

state charge density obtained from first-principles calculations in the presence of the CBC, which determines the electrostatic potential, will no longer be the “ground state” for the auxiliary system in which the CBC is removed. This unavoidable approximation has been discussed in previous works.^{50,51}

Once we have an expression for V_b , we can determine the energy associated with the interaction between the CBC and the slab, and also the self energy of the CBC; removing these energy contributions from the calculated energy of the supercell (as in Lozovoi *et al.*³¹) gives the corrected energy:

$$E_{es} = \tilde{E}_{es} - q\langle\tilde{V}\rangle + \frac{q}{2L_z} \int V_b(z)dz, \quad (8)$$

where $\langle\tilde{V}\rangle$ is the averaged electrostatic potential (a non-zero quantity), obtained from the first-principles calculation for the supercell, with the boundary conditions discussed above (see Fig. 3). $\langle\tilde{V}\rangle$, and thus the surface energy, depends on the ratio of the thickness of the slab to that of the vacuum region. This dependence is not spurious, but a reflection of the fact that the potential due to a charged surface diverges with distance from the surface. As will be demonstrated in Sec. IV C, the introduction of a reference electrode allows a consistent comparison of surface energies for equally sized cells with different amounts of charge.

For the case of a piecewise constant dielectric profile, we can substitute V_b from Eq. (7) into Eq. (8) and obtain

$$E_{es} = \tilde{E}_{es} - q\langle\tilde{V}\rangle - \frac{q^2}{24L_z\epsilon_0\Omega} \left(L_s^3 \left(1 - \frac{1}{\epsilon}\right) - L_z^3 \right). \quad (9)$$

3. Koopmans’ theorem for charged surfaces

To analyze the corrected energies, we use “Koopmans’ theorem for charged dielectric surfaces”, which is a generalization of “Koopmans’ theorem for charged metal surfaces” developed by Lozovoi *et al.*³¹ For a charged dielectric surface, the theorem states that the surface energy is given by

$$\gamma(q) = \gamma(0) + \phi\sigma + \frac{1}{\epsilon_0} \int_0^\sigma t \left[\frac{L_z}{2} - z_c(t) \right] dt, \quad (10)$$

where $\gamma(0)$ is the surface energy of the neutral slab; ϕ (a positive quantity in units of volts) is the potential difference between the vacuum level and the lowest unoccupied level (for electron addition) or the highest occupied level (for electron removal), calculated for the neutral dielectric surface; q is the total charge of the CBC (in units of electronic charge); σ is the surface charge density given by $\sigma = q/2A$, where A is the surface area per unit cell; $L_z/2$ is the position of the reference electrode; and z_c is the *centroid* of the excess surface charge given by,

$$z_c(\sigma) = \frac{1}{\sigma} \int_0^{\frac{L_z}{2}} z \delta\rho(\sigma; z) dz. \quad (11)$$

Here $\delta\rho(\sigma; z) = \rho(\sigma; z) - \rho_0(z)$, i.e., the excess surface charge is given as the difference between the planar averaged charge density of the charged surface calculation, $\rho(\sigma; z)$, and the planar averaged charge density of the neutral surface, $\rho_0(z)$. When presenting our results for surface energies we will use the explicit definition of z_c [Eq. (11)], but it is interesting to explore the sensitivity of the result to this value. Reassuringly, we will find in Sec. IV C that this sensitivity is low; i.e., if z_c is approximated to equal $L_s/2$ (the position of the surface layer in the neutral slab supercell), this results in only a small error in $\gamma(q)$.

The second term in Eq. (10) is the energy contribution of adding an electron to the lowest unoccupied state or removing it from the highest occupied state of the neutral slab with the electrodes serving as a reservoir of electrons. The third term is the energy of the electrostatic field in the parallel-plate capacitor formed between the electrode and the charge on the surface.

The term ‘‘Koopmans’ theorem’’ refers to the fact that the ionization energy, in the case of electron removal (or the electron affinity, in the case of electron addition) is given by the highest occupied molecular orbital (or the lowest unoccupied molecular orbital). Indeed, this is expressed by the second term of Eq. (10). We also note that, if we approximate z_c by $L_s/2$, all of the elements in Eq. (10) can be determined from a calculation for a neutral surface, justifying the name ‘‘Koopmans’ theorem for charged dielectric surfaces.’’ ‘‘Koopmans’ theorem for charged metal surfaces’’³¹ would be recovered by setting ϕ to the difference between the vacuum level and the Fermi level of the metallic surface.

III. ELECTRONIC STRUCTURE OF THE BULK AND SURFACE LaAlO_3

A. Bulk

LAO has a rhombohedral perovskite structure at room temperature and transforms into a cubic phase at ~ 813 K.⁴⁹ LAO has been observed to grow coherently in the cubic phase on cubic STO;^{27,52} therefore, we focus on cubic LAO in this study [Fig. 4(a)]. Since STO and LAO have a lattice mismatch of about 3%, LAO thin films grown on STO substrate might be strained. In our analysis, we neglect effects due to strain.

The electronic structure of LAO bulk calculated from first-principles is shown in Fig. 5. The valence-band maximum (VBM) at the R -point is composed mainly of O $2p$ states and the conduction-band minimum (CBM) at the Γ -point is composed mainly of doubly degenerate e_g La $5d$ states. The direct band gap of cubic LAO at the Γ -point is calculated to be 5.04 eV and the $R \rightarrow \Gamma$ indirect gap is 4.88 eV. Experimental data for the band gap of LAO is available only for the rhombohedral phase. Our calculated band gap for the rhombohedral phase is 5.51 eV, in good agreement with the observed value of 5.6

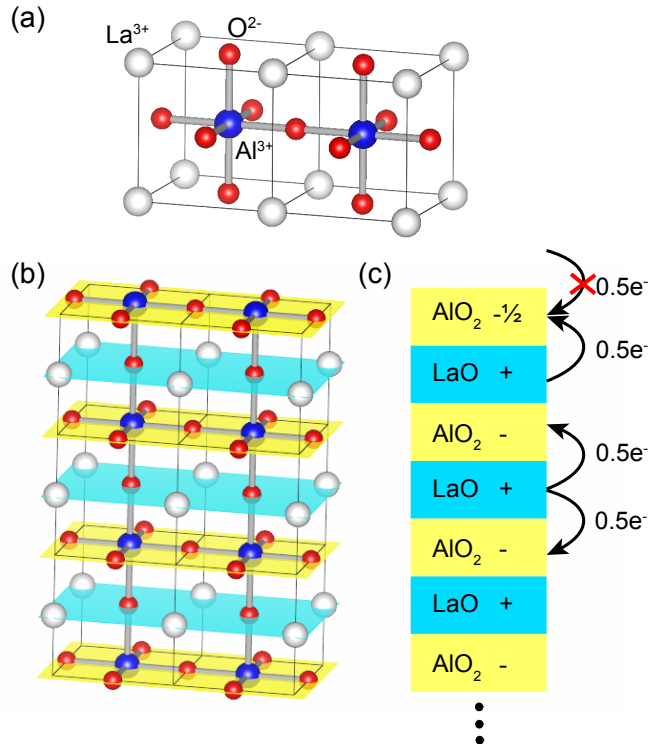


Figure 4. (Color online) (a) Schematic of the structure of cubic LAO, showing two unit cells with the AlO_6 octahedra. (b) Alternating layers of AlO_2 and LaO in a slab, with the surface terminating in an AlO_2 plane. (c) Schematic depicting interfacial charged planes and $0.5e^-$ electron transferred from LaO planes to the neighboring AlO_2 -planes in the bulk. The surface is shown terminated by an AlO_2 plane and lacks $0.5 e^-$.

eV.⁴⁹

B. Surface

Along the $[001]$ direction, LAO can be viewed as composed of alternating planes of LaO and AlO_2 , as shown in Fig. 4(b). In the ionic limit, the La and Al atoms each contribute 3 valence electrons, assuming a $+3$ charge, while O assumes a -2 charge. Thus, in the bulk an LaO plane ($\text{La}^{+3}\text{O}^{-2}$) has a net charge of $+1$ per unit cell, whereas an AlO_2 plane ($\text{Al}^{+3}\text{O}_2^{-2}$) has a charge of -1 per unit cell. Within this ionic picture, we can think of each LaO plane donating $0.5e^-$ per areal unit cell to the AlO_2 plane above and $0.5e^-$ to the AlO_2 plane below, as shown in Fig. 4(c).

At the surface, due to symmetry breaking along the $[001]$ direction, one of the two neighboring planes to an LaO or AlO_2 plane is absent, which leads to a deficit or excess of electrons at the surface. As illustrated in Fig. 4(c), the unreconstructed AlO_2 -terminated surface

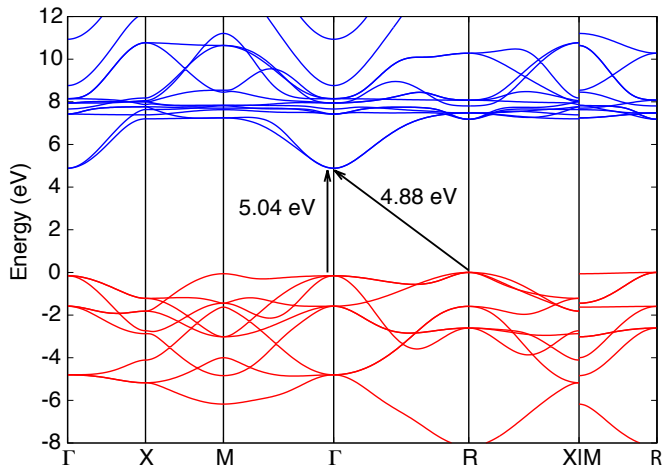


Figure 5. (Color online) Electronic structure of bulk cubic phase LAO. The direct (5.04 eV) and indirect (4.88 eV) band gaps are indicated. The zero of energy was set to the valence-band maximum at the R -point.

exhibits a deficit of $0.5 e^-$ (or, equivalently, an excess of 0.5 hole) per areal unit cell due to the lack of an LaO plane above to donate the electrons. Likewise, an unreconstructed LaO-terminated surface has an excess of $0.5e^-$ per unit-cell area due to the absence of an AlO_2 -plane above to accept the electrons.

The electronic structure of the AlO_2 - and LaO-terminated surfaces reflects the physics contained in this simple ionic picture. Figure 6 shows the calculated surface band structure of LAO projected onto the bulk valence and conduction bands. For the unreconstructed LaO-terminated surface, the band structure shown in Fig. 6(a) reveals surface states of La-5d character near the conduction band, partially filled with an excess of $0.5 e^-$ per areal unit, as expected from the ionic picture. On the other hand, for the unreconstructed AlO_2 -termination [Fig. 6(b)], surface states of O-2p character appear near the valence band, partially filled with 0.5 hole per areal unit.

We see that these surface structures lead to energetically unfavorable situations: occupied electron states occur near the conduction band for the LaO termination, or unoccupied states near the valence band for the AlO_2 termination. Overall these surfaces are expected to be unstable toward atomic reconstructions that fill low-lying states with electrons or remove electrons from high-lying states. In previous work,⁴¹ we calculated the surface energy of stable surface reconstructions for both the AlO_2 and LaO terminations for bulk LAO, assuming the surface to be charge neutral. The energy lowering obtained from surface reconstructions involving vacancies or adatoms can be explained with an electron-counting rule that assumes surface states in the upper part of the gap (i.e., with predominantly conduction-band character) should be unoccupied, and states low in the gap (with predominantly valence-band character)

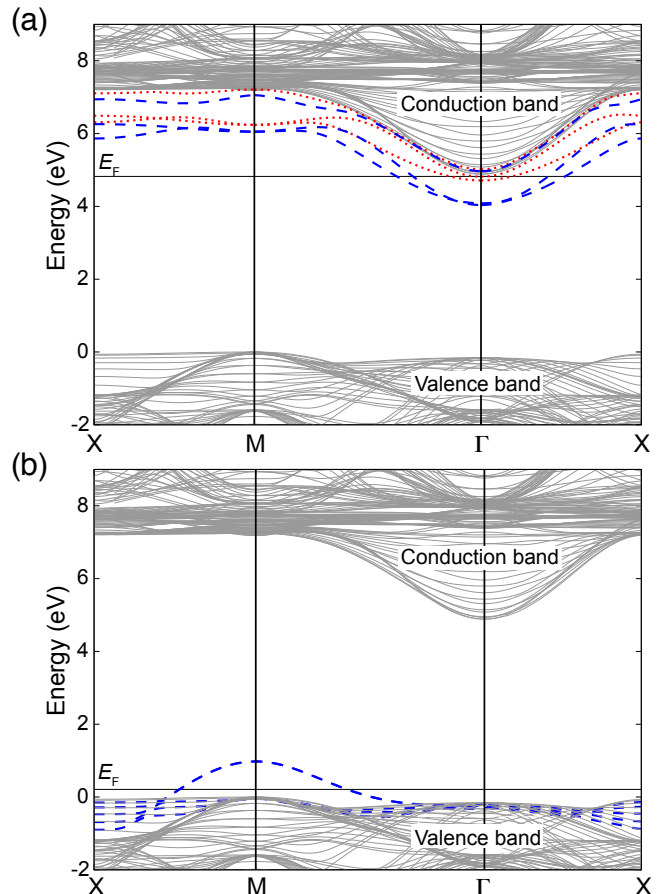


Figure 6. (Color online) Projected band structures for unreconstructed (but relaxed) (1×1) surfaces of LAO: (a) LaO-terminated and (b) AlO_2 -terminated. Solid (gray) curves represent projected bulk states. Dashed (blue) curves indicate spin-up (majority spin) surface states and dotted (red) curves represent spin-down surface states. For the AlO_2 -terminated surface in (b), spin-up and spin-down states are degenerate. The Fermi level E_F is indicated by horizontal solid (black) lines.

should be filled. In the following section, we address situations in which the electrons that fill the low-lying surface states on LAO are provided from another source, namely from the 2DEG at the LAO/STO interface, leading to a charged surface.

IV. SURFACE ENERGETICS OF LAO IN STO/LAO HETEROSTRUCTURES

Our situation of present interest, namely a thin layer of LAO on top of an STO substrate, provides a means for supplying charge to the surface. As described in Sec. III B, LAO can be viewed as alternating planes of AlO_2 and LaO, each with a charge of -1 and $+1$ per areal unit cell, respectively. A similar ionic picture for STO yields alternating layers of $(\text{Sr}^{+2}\text{O}^{-2})$ and $(\text{Ti}^{+4}\text{O}_2^{-2})$

with each layer being neutral. At the interface between LAO and STO, if the LAO terminates with an LaO plane and STO terminates with a TiO_2 plane forming a LaO- TiO_2 interface, the $0.5e^-$ per areal unit cell given up by the LaO plane transfers to the TiO_2 layer. Indeed, the TiO_2 layer does not require the excess electrons from the LaO plane for bonding, and the large conduction-band offset at the LAO/STO interface³⁹ ensures that the $0.5e^-$ per areal unit cell end up in the STO conduction band, giving rise to the 2DEG.

This argument is supported by our discussion of unreconstructed surfaces in Sec. III B, which provides direct insight in the electronic structure of the interface. For instance, the calculated electronic structure for the LaO-terminated surface [Fig. 6(a)], reveals the presence of excess electrons in surface states near the conduction band of LAO. If such a layer termination is interfaced with a nonpolar material such as STO, having a conduction band lower than that of LAO, the excess electrons end up occupying the conduction band of STO. Therefore, a 2DEG of density $\sim 3.3 \times 10^{14} \text{ cm}^{-2}$ corresponding to $0.5e^-$ per areal unit cell is intrinsic to the LaO- TiO_2 interface in the LAO/STO system.⁷

At the same time, if the actual surface of LAO in the LAO/STO heterostructure that is exposed to the surrounding environment terminates in an unreconstructed AlO_2 plane, the surface would have 0.5 holes per areal unit as in Fig. 6(b). These holes would serve as empty surface states that could be filled by electrons from the interfacial 2DEG transferring to the surface in order to minimize the total energy of the system. We are interested in quantifying the 2DEG density remaining at the interface after the transfer, that would minimize the total energy of the system for a certain thickness of LAO.

A. Reference structure

For our zero-energy reference structure, we choose an ideal LaO- TiO_2 interface between semi-infinite LAO and semi-infinite STO, which would have an intrinsic 2DEG completely confined near the interface (since the electrons have nowhere else to go), with a density corresponding to $0.5e^-$ per 2D unit cell ($3.3 \times 10^{14} \text{ cm}^{-2}$). Charge neutrality is satisfied because the density of the electrons in the 2DEG exactly equals the density of positive charges (0.5 positive charge per La atom) on the La atoms at the interface that have given up $0.5e^-$. The Fermi level is determined by the charge-neutrality equation, and will lie above the bottom of the STO conduction band in the region where the 2DEG occurs; see the band diagram in Fig. 7(a).

B. Neutral surfaces of LAO

Now we investigate what happens if the STO remains semi-infinite (corresponding to a bulk substrate), but the

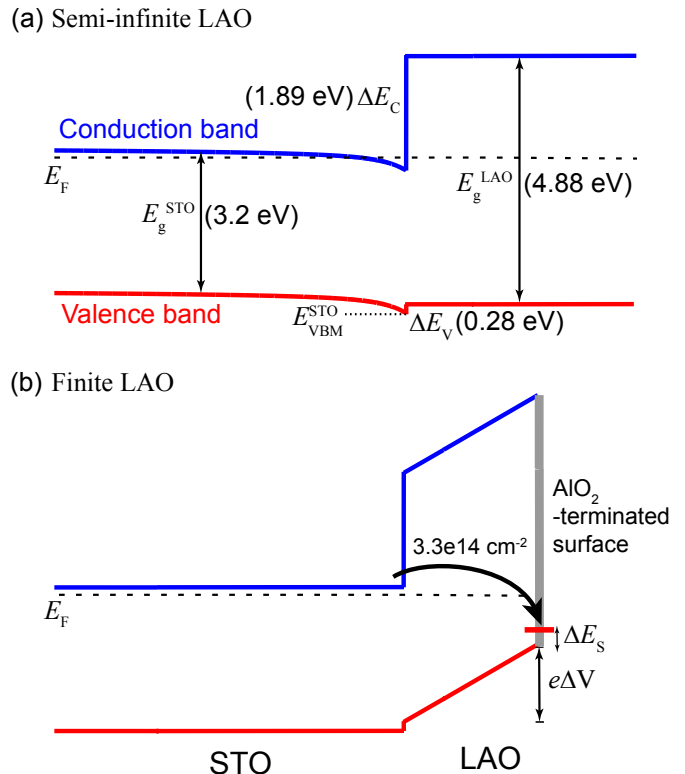


Figure 7. (Color online) Band diagram for the interface between semi-infinite SrTiO_3 and (a) semi-infinite LaAlO_3 showing band offsets and the formation of an intrinsic two-dimensional electron gas (2DEG), and (b) LaAlO_3 with a finite thickness less than the critical thickness, terminated by an AlO_2 plane containing surface states to which electrons from the 2DEG can transfer, leading to an insulating interface. The values for the band offsets are taken from Ref. 39.

LAO layer has a finite thickness; i.e., the LAO is terminated by a surface. Let us first consider the (hypothetical) situation in which we do not allow any charge transfer from the interface to the surface. The energy of this system would then simply correspond to the surface energy of the LAO. Using the methodology described in Sec. II B, we have calculated the absolute surface energy values for different surface reconstructions and terminations on bulk LAO. A full account is given in Ref. 41; here we summarize the key results and plot the calculated surface energy values for the unreconstructed as well as reconstructed surfaces for both LaO and AlO_2 terminations in Fig. 8.

The surface energy values in Fig. 8 depend on the chemical potentials of the constituent atoms, namely μ_{O} , μ_{Al} and μ_{La} , as in Eq. (1). These chemical potentials are representative of the chemical environment in which LAO is grown and characterized. We plot the surface energies as a function of μ_{O} , which is the variable that is most commonly controlled in experiments. The stability region of LAO [shaded regions in Fig. 8] is defined by these chemical potentials through Eq. (2), which forms

one constraint. Since there are three variables in total, we have to choose one additional constraint. As discussed in Sec. II B, we examine the two limits, namely Al-rich conditions [dashed boundary lines in Fig. 8], given by Eq. (3), and La-rich conditions [solid boundary lines in Fig. 8], given by Eq. (4). Once a limit is chosen, the surface energy becomes dependent on μ_O alone.

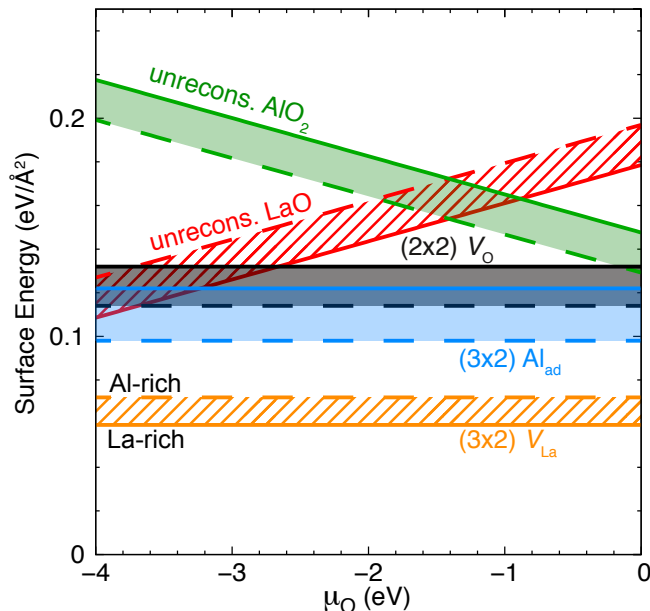


Figure 8. (Color online) Surface energy (in $\text{eV}/\text{\AA}^2$) for (2×2) O-vacancy (V_O) (black), (3×2) Al-adatom (Al_{ad}) (blue), and the (3×2) La-vacancy (V_{La}) (orange) reconstructions on the LaAlO_3 surface as a function of μ_O . The unreconstructed AlO_2 (green) and LaO (red) terminations are also shown. The regions shaded by diagonal crosshatching indicate the range of surface-energy values for LaO -terminated surfaces, and those shaded by solid colors are for AlO_2 -terminated surfaces, under the conditions within which LAO is stable; the boundaries indicated by dashed lines correspond to Al-rich conditions and those indicated by solid lines correspond to La-rich conditions. Details of stability regions and limiting conditions are discussed in the text.

Figure 8 illustrates that the surface energies of unreconstructed surfaces change linearly with μ_O , but that the surface energies of the reconstructed surfaces are independent of μ_O . The latter occurs because these particular surfaces are stoichiometric with respect to LAO , Al_2O_3 , and La_2O_3 . For the purposes of this paper, we will choose Al-rich conditions. A more comprehensive treatment, including a discussion of La-rich conditions, is included in Ref. 41.

The reconstructions that are found to be most stable are all consistent with the electron counting rule. For example, let us consider adding an Al adatom to the AlO_2 -terminated surface. The unreconstructed surface has 0.5 holes per areal unit cell [Sec. III B]. An Al adatom can donate 3 electrons. Therefore, an Al adatom every 6 areal

unit cells will result in an insulating state by completely filling all the holes. From the calculations, we indeed find a (3×2) Al-adatom reconstruction to be the most stable reconstruction on the AlO_2 termination, with the (2×2) O-vacancy slightly higher in energy. On the LaO termination, the (3×2) La-vacancy is the most stable reconstruction. Overall, the LaO termination with the (3×2) La-vacancy has the lowest surface energy, in the absence of impurities.

Our calculations also indicate that the presence of hydrogen alters the stability of the LaO versus the AlO_2 termination. Under Al-rich conditions, H binds to an O atom forming a (2×1) H-adatom reconstruction on the AlO_2 -terminated surface, whereas under La-rich conditions a (2×1) OH adsorbate reconstruction forms on the LaO -terminated surface.

C. Charged surfaces of LAO

In the previous section we considered an LAO layer of finite thickness on top of an STO substrate, and the (hypothetical) situation in which no charge transfer is allowed from the interface to the surface. Not allowing for charge transfer is unphysical, of course. For instance, as we saw in Sec. III B, the AlO_2 termination has unoccupied surface states in the lower part of the band gap, which lie well below the Fermi level (which is near the CBM of STO at the interface); based on the band alignment between STO and LAO (Fig. 7), we thus expect electron transfer from the interface to the surface. On the other hand, the LaO -terminated surface has no such empty states low in the gap [Fig. 6(a)], so no electron transfer will occur and the energy of the system with an LaO surface will remain unchanged. LaO -terminated surfaces would therefore be preferable from the point of view of maintaining a high density of electrons at the interface; however, such surfaces seem more difficult to obtain during thin-film growth.⁵² In the remainder of this section we focus on the AlO_2 -terminated surface.

In order to study the effect of charging the surface, we consider adding or removing electrons from the unreconstructed (1×1) AlO_2 -terminated surface. Our task will be to calculate the surface energy as a function of electrons added or removed. I.e., we wish to perform calculations on LAO slabs with (1×1) AlO_2 -terminated surfaces with various amounts of charge added to the cell using the supercell approach to treat charged surfaces as described in Sec. II C. We perform calculations with the surface charge ranging from -0.5 (addition of 0.5 electrons) to $+0.5$ (removal of 0.5 electrons, equivalent to addition of 0.5 holes) per 1×1 areal unit cell. This surface charge is related to the total CBC, q , as $-q/2A$, where A is the area of a unit cell and the factor of $\frac{1}{2}$ accounts for having two identical surfaces in the supercell. Figure 9 shows results for the total energy for different amounts of charge added to the supercell. The uncorrected surface energy (in $\text{meV}/\text{\AA}^2$) is obtained di-

rectly from the first-principles calculation, referenced to the corresponding neutral surface.

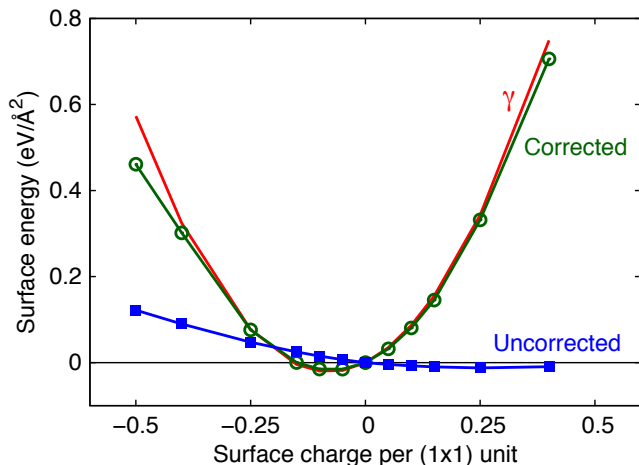


Figure 9. (Color online) Surface energy change (in $\text{eV}/\text{\AA}^2$) with respect to the neutral surface as a function of surface charge (in units of the magnitude of electronic charge) per (1×1) unit. Negative charge indicates added electrons and positive charge corresponds to electrons removed (or holes added). Solid squares (blue) are results without correction and open circles (green) represent corrected values. The solid (red) line shows the results of Eq. (10), based on Koopmans’ theorem generalized for charged surfaces.

As discussed in Sec. II C, the total energy (and hence the surface energy) obtained from a charged supercell calculation must be corrected for the spurious interaction due to the compensating background charge. We obtain the corrected surface energy by following the steps explained in Sec. II C leading to Eq. (9). The corrected energy corresponds to an auxiliary system where charge compensation is provided by reference electrodes placed at the edges of the supercell, and is also plotted in Fig. 9.

In order to analyze and disentangle the various energy contributions, we turn to the generalized “Koopmans’ theorem for charged dielectric surfaces” discussed in Sec. II C 3. According to the theorem, the energy of a charged surface of a dielectric upon the addition/removal of charge can be obtained solely from quantities related to the neutral surface, and is given by Eq. (10). We plot $\gamma(q)$ along with our uncorrected and corrected surface energies obtained from explicit charged-cell calculations in Fig. 9.

To ensure that the approximations made in Sec. II C are reasonable, we assess the sensitivity of the corrected surface energy values to the parameters being approximated. We performed these assessments for the case of $0.5 e^-$ per areal unit cell added, which can be considered a “worst case.” We explored different dielectric profiles, such as the error-function profile suggested by Komsa and Pasquarello,²⁸ but found that introducing a smearing of 1 \AA results in a change of less than $15 \text{ meV}/\text{\AA}^2$ in the corrected surface energy (which is small compared to the

magnitude of this energy, see Fig. 9). A 0.5 \AA change in the position of the surface plane, $L_s/2$, also changed the results by less than $15 \text{ meV}/\text{\AA}^2$. With regard to Eq. (10), we examined the case where z_c is assumed to be independent of the charge added. Taking $z_c = L_s/2$ resulted in an error of only $20 \text{ meV}/\text{\AA}^2$ in the surface energy $\gamma(q)$.

The approximate expression for $\gamma(q)$ [Eq. (10)] is remarkably very close to the results from our full first-principles calculations. We can therefore conclude that all of the changes in the surface energy due to charge addition are *extrinsic*, by which we mean that they result purely from the transfer of electrons between a reservoir of electrons (represented by the electrodes) and the surface. This *extrinsic* energy change can be separated into (1) the energy gained or lost due to the transfer of electrons between the reservoir at the vacuum level and the highest occupied/lowest unoccupied level on the surface [second term in Eq. (10)], and (2) an electrostatic contribution, which is equal to the energy required to charge a parallel-plate capacitor of separation equal to the vacuum thickness [third term in Eq. (10)].

Any deviation between the full, corrected result and the result based on Koopmans’ theorem must be attributed to *intrinsic* contributions, i.e., due to changes in the electronic structure of the surface upon charge addition. Our results indicate that these contributions are quite small, amounting to changes in the surface energy by less than $10 \text{ meV}/\text{\AA}^2$ for amounts of added charge up to a magnitude of about $0.4e^-$ per areal unit cell. This is small compared to the absolute value of the neutral AlO_2 -terminated surface energy, which is about $130 \text{ meV}/\text{\AA}^2$ (under Al-rich conditions at $\mu_O = 0 \text{ eV}$; see Fig. 8). Larger deviations in the surface energy occur for charge addition exceeding $0.4e^-$ per areal unit cell. We attribute this to electrons spilling out into the vacuum, which occurs due to the lowering of the potential in vacuum for such large CBC densities. This is actually an artifact of our first-principles calculations due to the presence of CBC in the vacuum region, and does *not* indicate that Koopmans’ theorem [Eq. (10)] is less accurate.

D. Energetics of LAO/STO with surface charging

We can now apply the general formalism for the surface-energy correction to the case of a thin layer of LAO on STO. We start from our zero-energy reference structure [Sec. IV A], which is the interface between semi-infinite LAO and semi-infinite STO, at which an intrinsic 2DEG with a density of $0.5e^-$ per 2D unit cell area ($3.3 \times 10^{14} \text{ cm}^{-2}$) is present [Fig. 7(a)].

When the thickness of LAO is finite, an energy cost needs to be paid associated with the creation of a surface. In the case of a neutral AlO_2 -terminated surface, and given our definition of the reference structure, this cost is simply equal to the surface energy for an unconstructed AlO_2 -terminated surface, $\gamma_{\text{AlO}_2}(\mu_O)$, which is shown in Fig. 8. But it is clear from Fig. 7 that the

energy can be lowered by transferring electrons from the 2DEG to unoccupied surface states on the surface, which in the case of the AlO_2 -terminated surface occur in the lower part of the band gap. This energy gain can be obtained from the approach discussed for LAO slabs in Sec. IV C: the surface-energy change is given by the energy related to the transfer of electrons from the electrode to the LAO surface. Within that formalism, the electrode acts as a reservoir for electrons, and its potential was set to zero. In a realistic LAO-STO system, which we are discussing now, the intrinsic 2DEG at the interface acts as the electron reservoir.

As charge is transferred between the 2DEG and the surface, a field builds up across the LAO layer, as shown in Fig. 7(b). This is the same type of field that was present in the vacuum, within the methodology for an isolated LAO slab discussed in Sec. IV C. This field contributes to the parallel-plate capacitor energy accounted for by the third term in Eq. (10). If we assume z_c to be constant (as discussed at the end of Sec. II C 3), then $(L_z/2 - z_c)$ is equivalent to the thickness d of the LAO layer. Equation (10) can then be rewritten for the specific case of LAO/STO, where the field is present across the LAO film, as

$$\begin{aligned} \gamma_{\text{AlO}_2}^{\text{LAO/STO}}(\mu_{\text{O}}) &= \gamma_{\text{AlO}_2}(\mu_{\text{O}}) - \\ \frac{\sigma_{\text{t}}}{e} [(E_{\text{F}} - E_{\text{VBM}}^{\text{STO}}) - \Delta E_v - \Delta E_s] + \frac{1}{2} \frac{\sigma_{\text{t}}^2 d}{\epsilon} & \quad (12) \\ &= \gamma_{\text{AlO}_2}(\mu_{\text{O}}) - \sigma_{\text{t}} \Delta V + \frac{1}{2} \frac{\sigma_{\text{t}}^2 d}{\epsilon} \end{aligned}$$

where $\gamma_{\text{AlO}_2}(\mu_{\text{O}})$ is the surface energy of the neutral AlO_2 -terminated surface [which depends on μ_{O} , see Sec. II B], σ_{t} is the charge density transferred from the interface to the surface, d is the LAO film thickness, and E_{F} , $E_{\text{VBM}}^{\text{STO}}$, ΔE_v , and ΔE_s are defined in Fig. 7. In the third line, we have combined these terms as $\Delta V = [(E_{\text{F}} - E_{\text{VBM}}^{\text{STO}}) - \Delta E_v - \Delta E_s]/e$, which is the potential change when an electron is transferred from the 2DEG to the surface states, analogous to the quantity ϕ in Eq. (10).

Comparing this expression to that developed by Bris-towe *et al.* [Eq. (16) in Ref. 9], we see that we have a very similar expression, but with opposite signs on the terms. The difference in the signs is due to the choice of the zero-energy reference structure, which in Ref. 9 is taken to be the LAO/STO structure with an insulating interface and a field in LAO. The energy that they derive is for electron-hole pairs being created and separated by the field to form the 2DEG and charge the surface. We, on the other hand take the 2DEG as intrinsic to the interface between semi-infinite LAO and semi-infinite STO, which is our zero-energy reference structure [Sec. IV A]. We feel our choice more accurately reflects the physics, and clearly identifies the origin of the electrons in the 2DEG.

Equation (12) shows that the surface energy depends on d and σ_{t} . Since there is an equal density of elec-

trons in the interfacial 2DEG and excess holes on the AlO_2 -terminated surface, there will be full transfer of electrons from the interface to the surface if the thicknesses d is small enough. The upper limit on this “small enough” thickness will be set by the situation where the surface states are raised high enough in energy to coincide with the Fermi level. This raising of the surface states occurs because of the presence of an electric field in the LAO layer. The field arises from the electron transfer, which leaves both the interface and the surface with a net charge, and can be calculated from Gauss’ law: $E = \sigma_{\text{t}}/\epsilon\epsilon_0$. For the case $\sigma_{\text{t}}/e = 3.3 \times 10^{14} \text{ cm}^{-2}$, using $\epsilon = 25$ [Ref. 53], this leads to a field $E = 2.4 \times 10^7 \text{ V/cm}$. The critical thickness is reached when the potential difference over the LAO layer, given by $E \cdot d$, becomes equal to ΔV (calculated to be 3.1 V), the difference between the Fermi level at the LAO/STO interface for the case of semi-infinite LAO (including band bending in STO due to the 2DEG), and the surface-state level E_s on the LAO surface; at that point the surface states are raised to the level of the Fermi level. This determines the maximum potential difference, because for larger values of d the electric field will be reduced by the transfer of electrons from the surface back to the interface. For a field $E = 2.4 \times 10^7 \text{ V/cm}$ and with $\Delta V = 3.1 \text{ V}$, the critical thickness is 1.3 nm (~ 3.5 unit cells), in agreement with the experimental value of 4 unit cells.

In general, for any given thickness d , the total charge transferred to the surface depends on ΔV as discussed above. Defining σ_{int} to be the intrinsic 2DEG density corresponding to $0.5e^-$ per areal unit, we can write σ_{t} as a function of d :

$$\sigma_{\text{t}} = \begin{cases} \frac{\Delta V \epsilon}{d}, & \Delta V \leq \frac{\sigma_{\text{int}} d}{\epsilon} \\ \sigma_{\text{int}}, & \Delta V \geq \frac{\sigma_{\text{int}} d}{\epsilon} \end{cases} \quad (13)$$

In Eq. (13), as the thickness of LAO becomes large ($d \rightarrow \infty$), the density of 2DEG electrons transferred to the surface becomes small ($\sigma_{\text{t}} \rightarrow 0$) with a $1/d$ dependence because the cost of transferring electrons to the surface becomes forbiddingly large. As a result, the 2DEG is restored back to the interface for very thick LAO.

V. SURFACE STABILITY AND ITS EFFECT ON 2DEG DENSITY

A. Unreconstructed AlO_2 -termination

The discussion in Sec. IV D shows that, for small thicknesses of LAO, the system with an unreconstructed but charged AlO_2 -terminated surface can significantly reduce its energy with respect to the neutral surface. In the present section we will address that energy lowering quantitatively, and also investigate whether the energy of the charged unreconstructed surface would become lower than the energy of reconstructed surfaces. The (corrected) surface energy for a 2-unit-cell thick LAO layer

with an AlO_2 -terminated surface is plotted in Fig. 10; the energy gained by charging the surface lowers the surface energy by $85 \text{ meV}/\text{\AA}^2$. We see that under O-rich conditions ($\mu_{\text{O}} \geq -1 \text{ eV}$) this charged surface is lower in energy than all of the reconstructed surfaces considered.

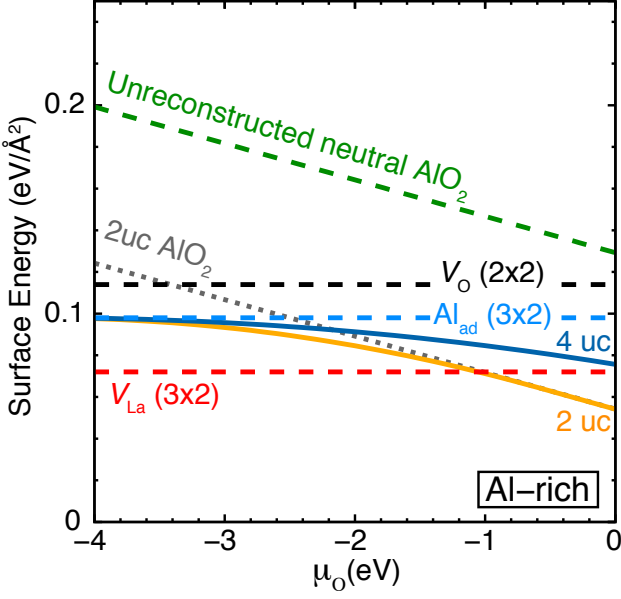


Figure 10. Surface energy (in $\text{eV}/\text{\AA}^2$) for AlO_2 -terminated thin films of LAO as a function of μ_{O} under Al-rich conditions [see Eq. (3)]. Results for an LaO-terminated surface with a (3×2) La-vacancy reconstruction are included for comparison. The dotted (gray) line labeled “2uc AlO_2 ” is the corrected surface energy after electron transfer to the unreconstructed AlO_2 -terminated surface for a 2-unit-cell LAO film. Solid lines refer to the minimized surface energy under a combination of electron transfer and an Al-adatom surface density of $C_{\text{Al}_{\text{ad}}}$ at each μ_{O} corresponding to a 2-unit-cell LAO film [light (orange) line] and a 4-unit-cell film [dark (blue) line]. The dashed lines refer to surface energies of (3×2) La-vacancy [$V_{\text{La}}(3 \times 2)$] (red), (2×2) O-vacancy [$V_{\text{O}}(2 \times 2)$] (black), and (3×2) Al-adatom [$\text{Al}_{\text{ad}}(3 \times 2)$] (blue) reconstructions, and the unreconstructed (but relaxed) AlO_2 -terminated surface (green).

B. Energetics due to surface defects and reconstructions

In Sec. IV, we considered the unreconstructed AlO_2 -terminated surface, and showed that charging the surface can significantly lower its energy, for small thicknesses of LAO films. The resulting energies need to be compared with those of the reconstructed surfaces; as discussed in Sec. IV B, reconstructions on neutral surfaces can also significantly reduce the surface energy.⁴¹ For the AlO_2 -terminated surface, the energetically favorable reconstructions are the ones that fill the holes in

surface states in the lower part of the band gap. For instance, Al adatoms act as donors, supplying 3 electrons per adatom; electron counting then indicates that a reconstruction consisting of one Al adatom in a 3×2 unit cell will exactly fill all the holes on the AlO_2 -terminated surface.

The result for a fully reconstructed $\text{Al}_{\text{ad}} 3 \times 2$ surface is included in Fig. 10. We observe that for μ_{O} values above -2.4 eV the energy of the charged surface (in the 2-uc case) is lower than that of the reconstructed $\text{Al}_{\text{ad}} 3 \times 2$ surface. However, in order to obtain a complete picture, we need to allow for the possibility that the filling of low-energy unoccupied surface states could result from a mixture of electron transfer and atomic reconstructions. Each Al adatom can compensate three holes on the surface. Energy is gained by filling the low-lying surface states, but there is a cost associated with the formation of the adatom “defects”. (We use the term “surface defects” here not to imply that we performed explicit calculations of surface point defects, but to refer to a uniformly spaced 2D array of a specific defect with a given concentration on the surface.) The process of forming a surface defect competes with the transfer of electrons from the 2DEG at the interface, which also has a cost, reflected in the third term of Eq. (12) (essentially the energy of a capacitor).

Let us assume we have donor defects of type i with a surface defect density C_i , which each contribute q_i electrons to the AlO_2 -terminated surface states. The sheet charge density of electrons transferred from the 2DEG to the surface, σ'_t , is now reduced because a fraction of the surface holes are compensated by the donor defects, leading to a modified version of Eq. (12):

$$\gamma_{\text{AlO}_2}^{\text{LAO/STO}}(\mu_{\text{O}}) = \gamma_{\text{AlO}_2}(\mu_{\text{O}}) - \sigma'_t \Delta V + \frac{1}{2} \frac{(\sigma'_t)^2 d}{\epsilon} + \sum_i \frac{C_i}{C_{\text{max}}} \Delta \gamma_i. \quad (14)$$

σ'_t is given by

$$\sigma'_t = \begin{cases} \frac{\Delta V \epsilon}{d}, & \Delta V \leq \frac{(\sigma_{\text{int}} - \sum_i C_i q_i) d}{\epsilon} \\ \sigma_{\text{int}} - \sum_i C_i q_i, & \Delta V \geq \frac{(\sigma_{\text{int}} - \sum_i C_i q_i) d}{\epsilon} \end{cases} \quad (15)$$

C_{max} is the defect density on the surface that would correspond to a completely reconstructed surface (i.e., completely filling the hole states) formed by the defect species; for instance, for Al adatom defects this corresponds to one Al adatom every six surface unit cells. $\Delta \gamma_i$ is the energy difference per areal unit between the completely reconstructed surface and the unreconstructed surface. Since energy is gained by forming the defect, $\Delta \gamma_i$ is a negative quantity. In our model, we approximate the surface energy in the presence of defects by a linear interpolation between the unreconstructed surface and the completely reconstructed surface formed by the defect. This allows us to obtain $\Delta \gamma_i$ from the calculated surface energies for a fully reconstructed surface (denoted

γ_i) compared to that of the unreconstructed surface:

$$\Delta\gamma_i = [\gamma_i(\mu_O) - \gamma_{\text{AlO}_2}(\mu_O)]. \quad (16)$$

Given a specific defect, and a thickness of LAO, our task will be to find the density of surface defects, and the 2DEG density remaining at the surface, that minimizes the energy of the system given by $\gamma_{\text{LAO/STO}}^{\text{LAO/STO}}(\mu_O)$ in Eq. (14). The constraint we impose for this minimization is the requirement that there are no empty states present on the surface in the lower part of band gap; i.e., all the holes on the surface are completely filled either by electrons transferred from the 2DEG or by electrons donated by surface defects.

C. Effect of surface defects and reconstructions on the 2DEG density

We now investigate the effect of surface reconstructions and defects on thin LAO films and the 2DEG density at the interface. As discussed earlier, the formation of these defects cause a reduction in the available surface states because of their donor nature. Due to this, there will now be fewer electrons, σ_t' transferring to the surface from the interface, in comparison to the case where there are no such surface defects, for a given thickness d . The effect of these surface defects will be to alter the 2DEG density at the interface from the intrinsic density value, σ_{int} . Therefore, the resulting 2DEG density at the interface is given by $(\sigma_{\text{int}} - \sigma_t')$. For a specific surface defect, our task will be to determine σ_t' , for a given thickness d , which minimizes the energy of the LAO/STO system (compared to our zero-energy reference system) given in Eq. (14). As a consequence, we also determine the density of surface defects, C_i that also simultaneously minimizes the energy in Eq. (14) for a given d .

Oxygen vacancies as surface defects have been extensively discussed in the literature [Ref. 9 and references therein]. Our own calculations indicate, however, that Al adatoms (Al_{ad}) in a 3×2 configuration are more stable for all experimental growth conditions than O-vacancies (V_{O}) in a 2×2 configuration⁴¹ [Fig. 8]. In addition, it may be necessary to consider adsorption of impurities. In particular, hydrogen is present in most growth and annealing environments. We therefore also consider the effect of H adatoms on the 2DEG density. Indeed, from our previous calculations⁴¹ we found that H adatoms (H_{ad}) serve as donors on the AlO_2 -termination by completely filling the holes on the surface and forming a (2×1) surface reconstruction. In the following analysis, we focus on these specific surface defects, namely Al_{ad} , V_{O} and H_{ad} , and study their effect on the surface energies of the AlO_2 -terminated surface and the resulting 2DEG densities at the interface.

The number of electrons donated by a specific defect is obtained from the charge state of the defect. An Al_{ad} donates $3e^-$. Therefore, for any given surface density of

Al_{ad} , $C_{\text{Al}_{\text{ad}}}$, the sheet density of empty states on the surface, which can take up electrons, can be determined. In practice, to determine $C_{\text{Al}_{\text{ad}}}$ that minimizes the energy of the LAO/STO structure, we calculate the energy in Eq. (14) at different values for $C_{\text{Al}_{\text{ad}}}$, for a given thickness and fixed chemical potentials (for example $\mu_O = 0$ eV) with the constraint that the holes in surface states are completely filled either by electrons donated by surface defects or by electrons transferred from the 2DEG or a combination of both. The minimum of the surface energies computed determines $C_{\text{Al}_{\text{ad}}}$, as well as the resulting 2DEG density at the interface ($\sigma_{\text{int}} - \sigma_t'$), for a given d and chemical potential. The minimized values for the surface energy in the presence of Al-adatom defects for 2- and 4-unit-cell thick LAO are plotted as a function μ_O in Fig. 10. We see that for these thicknesses, it is more favorable to transfer electrons to the surface under O-rich conditions. As we move towards O-poor conditions, $C_{\text{Al}_{\text{ad}}}$ increases, tending towards the value corresponding to the (3×2) reconstruction under extremely O-poor conditions.

The resulting 2DEG density is plotted as a function of thickness d for two oxygen chemical-potential values, $\mu_O = 0$ eV (O-rich conditions) [Fig. 11(a)] and $\mu_O = -2$ eV (O-poor conditions) [Fig. 11(b)]. Due to the constraint imposed on the surface to be insulating, as holes in LAO surface states are energetically unfavorable, the density of Al adatoms on the surface, $C_{\text{Al}_{\text{ad}}}$, exhibits the same trend with thickness as does the 2DEG density at the interface. A treatment for V_{O} leads to similar trends in the 2DEG density with thickness, as plotted in Fig. 11. Each V_{O} donates $2e^-$. For both Al_{ad} and V_{O} the critical thickness and the 2DEG density strongly depend on the oxygen chemical potential μ_O , with O-rich conditions favoring a higher 2DEG density.

Results for H_{ad} , which donates $1e^-$, are also included in Fig. 11. Since the energy of surfaces with H_{ad} depends on the hydrogen chemical potential μ_{H} , in addition to its dependence on oxygen chemical potential μ_O , we present results for two cases: $\mu_{\text{H}} = -1$ eV (H-rich), and $\mu_{\text{H}} = -2$ eV (H-poor). The critical thickness and the 2DEG density are strongly altered by the hydrogen chemical potential, with H-rich conditions giving a higher 2DEG density. We note, however, that the 2DEG density for H_{ad} is independent of μ_O . This is because the AlO_2 -terminated surface with H adatoms has the same stoichiometry as an unreconstructed AlO_2 -terminated surface, which leads to an identical dependence on μ_O for $\gamma_{\text{H}_{\text{ad}}}(\mu_O)$ and $\gamma_{\text{AlO}_2}(\mu_O)$. Therefore, the energy gain in Eq. (16) becomes independent of μ_O . The 2DEG density in the absence of surface defects is also plotted in Fig. 11 for comparison. It can be seen that the presence of surface defects increases the 2DEG density and alters the critical thickness required to form the 2DEG. These trends are consistent with experimental observations by Xie *et al.*^{15,17,18} They observed that increasing the exposure of the surface to adsorbates modulates the 2DEG density, and for certain cases even switches the interface

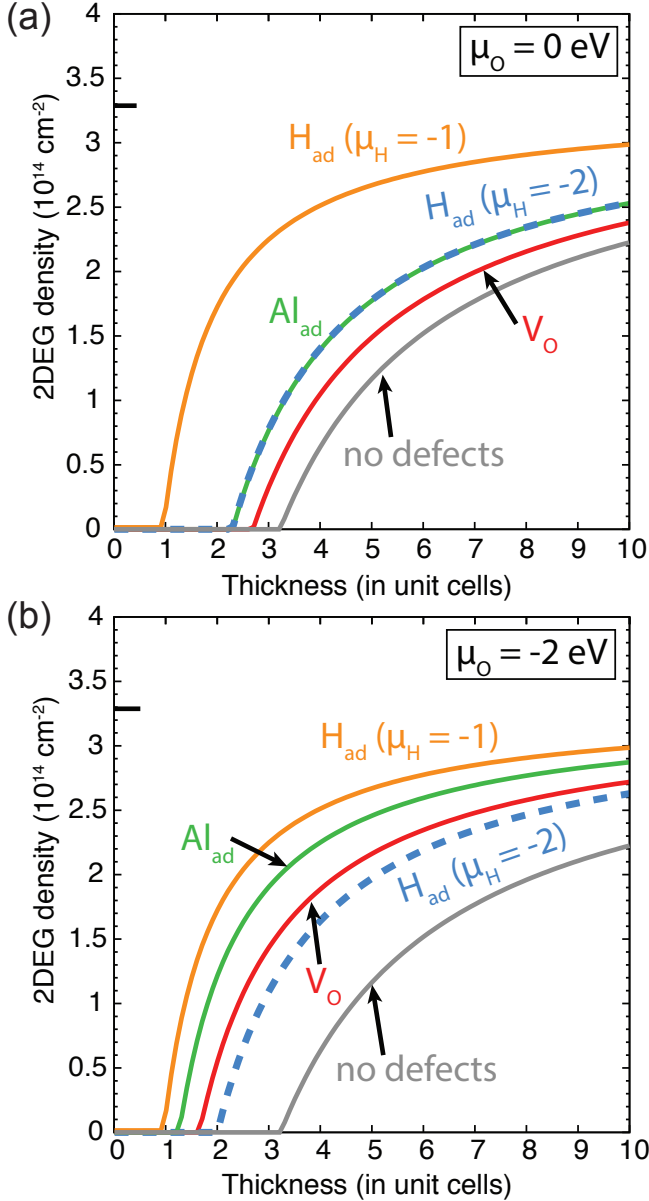


Figure 11. 2DEG density (in units of 10^{14} cm^{-2}) under Al-rich conditions as a function of LAO thickness for different surface defects, namely, Al-adsorbate (Al_{ad}) (green), O-vacancy (V_{O}) (red), and H-adsorbate (H_{ad}) for $\mu_{\text{H}} = -1 \text{ eV}$ (solid orange) and for $\mu_{\text{H}} = -2 \text{ eV}$ (dotted blue) at (a) $\mu_{\text{O}} = 0 \text{ eV}$, and (b) $\mu_{\text{O}} = -2 \text{ eV}$. For comparison, the 2DEG density in the absence of surface defects is plotted in gray (labeled “no defects”). The maximum 2DEG density corresponding to $3.3 \times 10^{14} \text{ cm}^{-2}$ is indicated by the black horizontal bar.

from an insulating to a conductive state. This is due to the strong influence of the exposure conditions on the adsorbate density on LAO.

Our calculated values for the 2DEG densities and for the critical thickness are in qualitative agreement with the majority of experimental reports;^{4,13–19,54} however, quantitative agreement is still lacking. One reason for

the discrepancies might be the sensitivity of the results to the value of the dielectric constant. We used $\epsilon = 25$ [Ref. 53], but ϵ is known to be dependent on strain and electric field, as noted by Chen *et al.*²⁵ Values ranging from 21 to 46 have been used in the literature,^{8,9,25} recognizing that the critical thickness and the 2DEG density are sensitive to ϵ . We also note that there is a lack of agreement between different experimental methods of measuring the 2DEG density; specifically, transport and optical measurements give different results.⁵⁵ The experimentally reported 2DEG densities obtained for different samples vary by an order of magnitude. Our aim in the present work was to comprehensively address the effects of the LAO surface on the 2DEG density. We are confident that the trends obtained from our analysis are correct and informative. However, the actual 2DEG density probed by experiments can be affected by a number of other mechanisms, such as carrier localization, defect-related trapping centers, and stoichiometry. These effects are beyond the scope of the present paper, but could be readily incorporated into the general model we have developed. Specifically, our model can be extended to various surface processes that might occur on the LAO surface, and can be used to explore heterostructures other than LAO/STO.

VI. CONCLUSIONS

We have outlined a general methodology for addressing the commonly occurring problem in surface science where there is an exchange of charge between the surface and a source/sink of charge within the system. This includes semiconductor surfaces, where exchange of charge between an interface or dopants/defects near the surface (reservoir) and surface states gives rise to band bending. Instead of performing first-principles calculations on the complete system (including the surface as well as the reservoir), which is often computationally prohibitive, our approach allows us to treat the surface in isolation and simultaneously take the charge exchange into account by way of charged surface calculation, thereby greatly reducing the computational cost involved. In order to assess the surface energetics for such charged surfaces we developed a methodology for charged dielectric surfaces.

Equipped with this methodology, we have addressed LAO/STO heterostructures and established a consistent model that describes the 2DEG formation as well as charge transfer and interactions between the 2DEG and the LAO surface. Quantitative results were obtained using first-principles calculations based on hybrid density functional theory. A 2DEG of density $3.3 \times 10^{14} \text{ cm}^{-2}$ is intrinsic to the LaO-TiO₂-type interface. However, in the presence of an LAO surface, the electrons from the 2DEG may transfer to surface states leaving the interface insulating or with a smaller 2DEG density. In particular, an AlO₂-terminated surface exhibits empty states near the

valence band that can be filled by the 2DEG electrons. Indeed, we find that filling these surface states stabilizes the AlO₂-termination significantly, and provides an explanation for the observed insulating behavior of samples below a certain critical thickness.²⁻⁴

We also allowed for the presence of defects on the surface. Using first-principles values for surface energies, we then obtained the 2DEG density as a function of thickness of the LAO layer. We find that the critical thickness required to form the 2DEG is sensitive to the oxygen chemical potential (as well as the hydrogen chemical potential, in case of hydrogen being present in the environment), and that increasing the surface defect density

reduces the critical thickness.

ACKNOWLEDGEMENTS

The authors thank H. Komsa and A. Pasquarello for fruitful interactions about corrections for charged surfaces. This work was supported in part by the Center for Low Energy Systems Technology (LEAST), one of six SRC STARnet Centers sponsored by MARCO and DARPA, and by the U. S. Army Research Office under grant number W911-NF-11-1-0232. Computing resources were provided by the CSC/CNSI/MRL (an NSF MRSEC, DMR-1121053), supported by NSF CNS-0960316, and by XSEDE, supported by NSF ACI-1053575.

-
- ¹ A. Ohtomo and H. Y. Hwang, *Nature* **427**, 423 (2004).
² S. Thiel, G. Hammerl, A. Schmehl, C. W. Schneider, and J. Mannhart, *Science* **313**, 1942 (2006).
³ A. Brinkman, M. Huijben, M. van Zalk, J. Huijben, U. Zeitler, J. C. Maan, W. G. van der Wiel, G. Rijnders, D. H. A. Blank, and H. Hilgenkamp, *Nature Mater.* **6**, 493 (2007).
⁴ S. Gariglio, N. Reyren, A. D. Caviglia, and J.-M. Triscone, *J. Phys.: Condens. Matter* **21**, 164213 (2009).
⁵ N. Nakagawa, H. Y. Hwang, and D. A. Muller, *Nature Mater.* **5**, 204 (2006).
⁶ Y. Segal, J. H. Ngai, J. W. Reiner, F. J. Walker, and C. H. Ahn, *Phys. Rev. B* **80**, 241107 (2009).
⁷ A. Janotti, L. Bjaalie, L. Gordon, and C. G. Van de Walle, *Phys. Rev. B* **86**, 241108 (2012).
⁸ N. C. Bristowe, P. B. Littlewood, and E. Artacho, *Phys. Rev. B* **83**, 205405 (2011).
⁹ N. C. Bristowe, P. Ghosez, P. B. Littlewood, and E. Artacho, *J. Phys.: Condens. Matter* **26**, 143201 (2014).
¹⁰ W.-J. Son, E. Cho, J. Lee, and S. Han, *J. Phys.: Condens. Matter* **22**, 315501 (2010).
¹¹ R. Arras, V. G. Ruiz, W. E. Pickett, and R. Pentcheva, *Phys. Rev. B* **85**, 125404 (2012).
¹² C. Cen, S. Thiel, G. Hammerl, C. W. Schneider, K. E. Andersen, C. S. Hellberg, J. Mannhart, and J. Levy, *Nature Mater.* **7**, 298 (2008).
¹³ F. Bi, D. F. Bogorin, C. Cen, C. W. Bark, J.-W. Park, C.-B. Eom, and J. Levy, *Appl. Phys. Lett.* **97**, 173110 (2010).
¹⁴ Y. Xie, C. Bell, T. Yajima, Y. Hikita, and H. Y. Hwang, *Nano Lett.* **10**, 2588 (2010).
¹⁵ Y. Xie, Y. Hikita, C. Bell, and H. Y. Hwang, *Nat. Commun.* **2**, 494 (2011).
¹⁶ A. Kumar, T. Arruda, Y. Kim, and I. Ivanov, *ACS Nano* **6**, 3841 (2012).
¹⁷ Y.-W. Xie and H. Y. Hwang, *Chin. Phys. B* **22**, 127301 (2013).
¹⁸ Y. Xie, C. Bell, Y. Hikita, S. Harashima, and H. Y. Hwang, *Adv. Mater.* **25**, 4735 (2013).
¹⁹ C. Bark, P. Sharma, Y. Wang, and S. Baek, *Nano Lett.* **12**, 1765 (2012).
²⁰ T. C. Asmara, A. Annadi, I. Santoso, P. K. Gogoi, A. Kotlov, H. M. Omer, M. Motapothula, M. B. H. Breese, M. Rübhausen, T. Venkatesan, Ariando, and A. Rusydi, *Nat. Commun.* **5**, 3663 (2014).
²¹ After submission of the present work we became aware of the following publication: O. Sinai, O. T. Hofmann, P. Rinke, M. Scheffler, G. Heimel and L. Kronik, *Phys. Rev. B* **91**, 075311 (2015).
²² M. Stengel, *Phys. Rev. Lett.* **106**, 136803 (2011).
²³ F. Cossu, U. Schwingenschlögl, and V. Eyert, *Phys. Rev. B* **88**, 045119 (2013).
²⁴ A. Sorokine, D. Bocharov, S. Piskunov, and V. Kashcheyevs, *Phys. Rev. B* **86**, 155410 (2012).
²⁵ H. Chen, A. M. Kolpak, and S. Ismail-Beigi, *Adv. Mater.* **22**, 2881 (2010).
²⁶ L. Yu and A. Zunger, *Nat. Commun.* **5**, 5118 (2014).
²⁷ S. Chambers, M. Engelhard, V. Shutthanandan, Z. Zhu, T. Droubay, L. Qiao, P. Sushko, T. Feng, H. Lee, T. Gustafsson, E. Garfunkel, A. Shah, J.-M. Zuo, and Q. Ramasse, *Surf. Sci. Rep.* **65**, 317 (2010).
²⁸ H.-P. Komsa and A. Pasquarello, *Phys. Rev. Lett.* **110**, 095505 (2013).
²⁹ W. Mönch, *Semiconductor Surfaces and Interfaces* (Springer Science & Business Media, New York, NY, USA, 2001) p. 59.
³⁰ N. A. Richter, S. Siculo, S. V. Levchenko, J. Sauer, and M. Scheffler, *Phys. Rev. Lett.* **111**, 045502 (2013).
³¹ A. Y. Lozovoi, A. Alavi, J. Kohanoff, and R. M. Lynden-Bell, *J. Chem. Phys.* **115**, 1661 (2001).
³² J. Heyd, G. E. Scuseria, and M. Ernzerhof, *J. Chem. Phys.* **118**, 8207 (2003).
³³ J. Heyd, G. E. Scuseria, and M. Ernzerhof, *J. Chem. Phys.* **124**, 219906 (2006).
³⁴ P. E. Blöchl, *Phys. Rev. B* **50**, 17953 (1994).
³⁵ G. Kresse and D. Joubert, *Phys. Rev. B* **59**, 1758 (1999).
³⁶ G. Kresse and J. Hafner, *Phys. Rev. B* **47**, 558 (1993).
³⁷ G. Kresse and J. Furthmüller, *Comp. Mater. Sci.* **6**, 15 (1996).
³⁸ G. Kresse and J. Furthmüller, *Comp. Mater. Sci.* **6**, 15 (1996).
³⁹ L. Bjaalie, B. Himmetoglu, L. Weston, A. Janotti, and C. G. Van de Walle, *New J. Phys.* **16**, 025005 (2014).
⁴⁰ A. Janotti, D. Steiauf, and C. G. Van de Walle, *Phys. Rev. B* **84**, 201304 (2011).

- ⁴¹ K. Krishnaswamy, C. E. Dreyer, A. Janotti, and C. G. Van de Walle, *Phys. Rev. B* **90**, 235436 (2014).
- ⁴² H. Monkhorst and J. Pack, *Phys. Rev. B* **13**, 5188 (1976).
- ⁴³ C. Freysoldt, J. Neugebauer, and C. G. Van de Walle, *Phys. Rev. Lett.* **102**, 016402 (2009).
- ⁴⁴ C. Freysoldt, J. Neugebauer, and C. G. Van de Walle, *Phys. Status Solidi B* **248**, 1067 (2011).
- ⁴⁵ C. Freysoldt, B. Grabowski, T. Hickel, J. Neugebauer, G. Kresse, A. Janotti, and C. G. Van de Walle, *Rev. Mod. Phys.* **86**, 253 (2014).
- ⁴⁶ J. Lee and A. A. Demkov, *Phys. Rev. B* **78**, 193104 (2008).
- ⁴⁷ Y. Li and J. Yu, *J. Phys. Condens. Matter* **25**, 265004 (2013).
- ⁴⁸ A. Baldereschi, S. Baroni, and R. Resta, *Phys. Rev. Lett.* **61**, 734 (1988).
- ⁴⁹ S.-G. Lim, S. Kriventsov, T. N. Jackson, J. H. Haeni, D. G. Schlom, A. M. Balbashov, R. Uecker, P. Reiche, J. L. Freeouf, and G. Lučovský, *J. Appl. Phys.* **91**, 4500 (2002).
- ⁵⁰ M. Leslie and N. Gillan, *J. Phys. C Solid State Phys.* **18**, 973 (1985).
- ⁵¹ G. Makov and M. C. Payne, *Phys. Rev. B* **51**, 4014 (1995).
- ⁵² M. Huijben, G. Rijnders, D. H. A. Blank, S. Bals, S. Van Aert, J. Verbeeck, G. Van Tendeloo, A. Brinkman, and H. Hilgenkamp, *Nature Mater.* **5**, 556 (2006).
- ⁵³ X.-b. Lu, Z.-g. Liu, Y.-p. Wang, Y. Yang, X.-p. Wang, H.-w. Zhou, and B.-y. Nguyen, *J. Appl. Phys.* **94**, 1229 (2003).
- ⁵⁴ Y. Yamada, H. K. Sato, Y. Hikita, H. Y. Hwang, and Y. Kanemitsu, *Appl. Phys. Lett.* **104**, 151907 (2014).
- ⁵⁵ G. Berner, S. Glawion, J. Walde, F. Pfaff, H. Hollmark, L.-C. Duda, S. Paetel, C. Richter, J. Mannhart, M. Sing, and R. Claessen, *Phys. Rev. B* **82**, 241405 (2010).